Proc. 11th New Zealand Geothermal Workshop 1989

THE CORROSIVITY, SILICA AND CALCITE DEPOSITION TENDENCIES OF THE DARAJAT GEOTHERMAL FLUIDS, WEST JAVA

Rizal Astrawinata

Jur. Teknik Pertambangan - Fakultas Teknologi Mineral
Institut Teknologi Bandung
Indonesia

ABSTRACT

The objective of this study was to determine the corrosiveness and the deposition tendency of the Darajat geothermal fluids. It is essential to have some measure of the corrosivity and the strength of the scaling tendency if the exploitability of the Darajat field is to be evaluated from a materials point of view.

INTRODUCTION

A good understanding of the corrosive environment and deposition tendency of the fluids in a geothermal field is essential in determining if the field is exploitable for geothermal fluid energy recovery. To evaluate the exploitability of a new and unexploited geothermal field from a materials point of view some measure of surface corrosion and cracking susceptibility of "standard" engineering materials, as well as the scaling tendency of the geothermal fluids is necessary. The purpose of this study is to establish a knowledge of the corrosivity and to assess the scaling tendency of the Darajat geothermal fluids in West Java, Indonesia. To achieve these objectives, a simple series of materials testing procedures have been conducted to measure surface corrosion rates, to check for stress-enhanced corrosion and to determine scaling tendency.

To assess surface corrosion, electrical resistance technique and weight-loss method have been chosen. For the evaluation of stress-enhanced corrosion, u-bend specimens were used. Since scaling tendency of the geothermal fluids is intimately associated with the fluid chemistry, analysis using solubility diagrams based on the chemical composition of the fluids were conducted. Perforated scale coupons were also incorporated in the test to monitor the strength of the scaling tendency.

Because different phases of the geothermal fluids exhibit different chemical composition, each phase can result in different corrosivity and deposition tendency. In this study four different types of Darajat geothermal media were assessed, namely: the raw steam, the liquid phase separated from the steam, the steam condensate, and the aerated steam condensate.

The obtained results are intended not only to assist in the evaluation of the exploitability of the Darajat geothermal field but also to provide additional information as a contribution to the existing geothermal database.

THE CHEMISTRY OF THE GEOTHERMAL FLUIDS

The first step in considering the corrosiveness and the deposition tendency of geothermal fluids is to evaluate the chemistry of the fluids. During the period of September 1988 through November 1988 thirteen samples of the liquid phase separated from the steam (separated water) and the liquid phase condensed from the separated steam (steam condensate) were taken and analyzed. The average compositions of these geothermal fluids are presented in Table-1.

An important tool in the analysis of the corrosion and deposition phenomena in geothermal fluids is equilibrium thermodynamics. The complexity of such problems dictates that the thermodynamic analysis be represented in graphical forms. It is important to realize that the derived diagrams are valid only for the species considered, and that the final diagram will not reveal whether species that are not considered might be stable to those used. Care must also be exercised in the interpretation and use of these diagrams because of the possible ommision of a relevant species. And finally the validity of these diagrams will hinge on the reliability of the thermodynamic data employed.

To determine the corrosion chemistry of the geothermal fluids, potential-pH diagrams for $Fe\text{-}H_2O\text{-}S$ systems were drawn. These Eh-pH diagrams are based on the data of Table-1 and collected thermodynamic data available in the literatures. The diagrams describe the equilibrium corrosion reactions of pure iron in contact with the geothermal fluids at the specified temperatures. The potential-pH diagram for the separated water at 150° C is illustrated in Figure-1, while the one for the steam condensate at 50° C is given in Figure-2. The diagrams indicate that, at the specified averaged values of pH for each medium, the corrosion product formed in the separated water would likely be FeS_2 or Fe_2O_3 while in the steam condensate ferrous ion or $Fe(OH)_3$ may probably be formed. In addition, the diagram also revealed that at the given pH values, the stability region of elemental sulphur is insignificant, i.e., sulphur deposition is not likely to occur.

In treating the equilibrium thermodynamics describing calcium carbonate deposition, it is important to distinguish two cases:

1. systems that are closed to the atmosphere
2. systems that include a gas phase at a given partial pressure of gaseous CO_2 in addition to the solid and solution phase.

Because of its significance in natural water system, calcite will represent the solid phase in these two cases.

In the closed system the carbonic acid is treated as a nonvolatile acid, including also

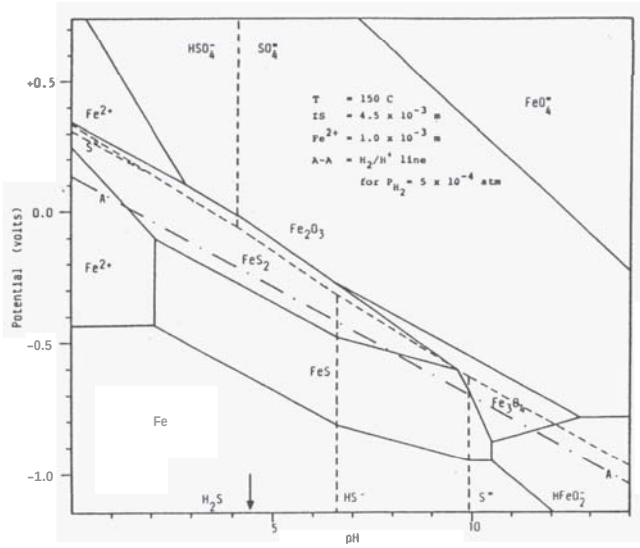

Figure–1: Potential–pH diagram of Fe–H_2O–S system for separated water at 150" C.

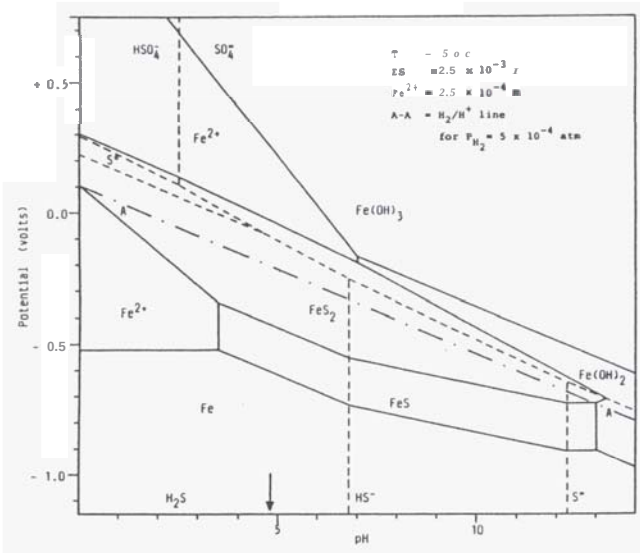

Figure–2: Potential–pH diagram of Fe–H–O–S system for steam condensate at 50" C.

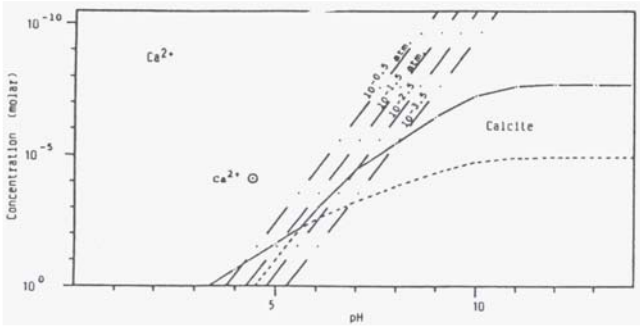

Figure–3: Solubility of calcite in the separated water at 150° C.

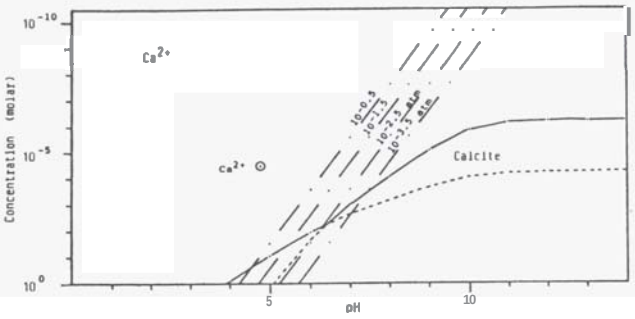

Figure–4: Solubility of calcite in the steam condensate at 50' C.

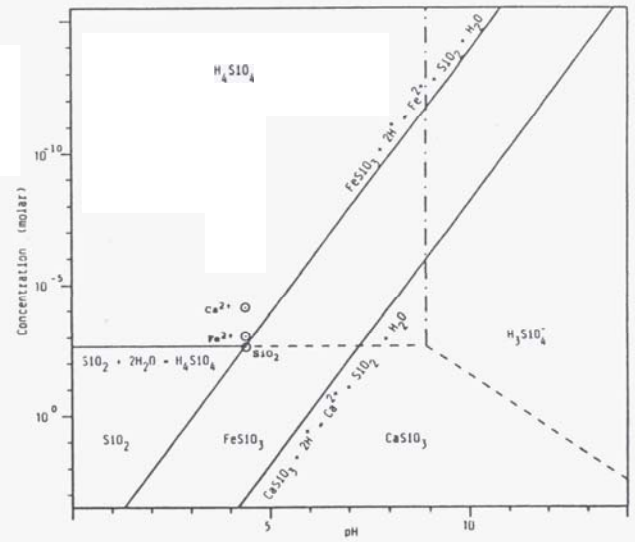

Figure–5: Solubility of silica, iron and calcium silicate in the separated water at 150' C.

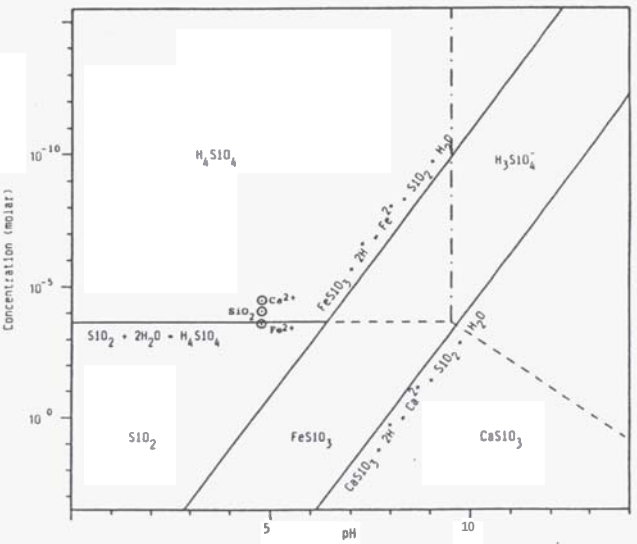

Figure–6: Solubility of silica, iron and calcium silicate in the steam condensate at 50" C.

all the dissolved CO_2. Furthermore, one must consider the saturation condition of calcite (i) if the concentration of calcium ions in the solution equals to the concentration of all dissolved carbonic species, and (ii) if the solution contains a fixed quantity of carbonic species.

For the system in equilibrium with gaseous CO_2, partial pressures of CO_2 are selected ranging from $10^{-0.5}$ atm. to $10^{-3.5}$ atm., the latter of which is the partial pressure of CO_2 in equilibrium with the atmosphere.

The solubility of calcite as a function of pH for the separated water and for the steam condensate are given in Figure-3 and Figure-4, respectively. These diagrams indicate the stability region of calcium ions and of calcite. It can be seen that, at the averaged pH values, the separated water and the steam condensate are undersaturated with calcium ions implying that the probability of calcite deposition is unlikely.

The solubility evaluation of silica is quite important in estimating the precipitation of various silicate minerals from high temperature water. Unfortunately pertinent thermodynamic data are not known with any precision and the uncertainties make the analysis of a detailed thermodynamic consideration uncertain. However, by using best available thermodynamic data, stability diagrams that may help in understanding the precipitation of silica as well as of iron and calcium containing silicate minerals can be constructed. Figure-5 and Figure-6, respectively, depict the stability diagrams of silica, $FeSiO_3$ and $CaSiO_3$ for the separated water and the steam condensate of the Darajat geothermal fluids.

At the averaged value of pH = 4.5, Fig.-5 shows that the separated water is saturated with ferrous ions and silicic acid capable of precipitating $FeSiO_3$ and SiO_2 deposits. On the other hand, the fluid is undersaturated with calcium ions to precipitate $CaSiO_3$. Figure-6 indicate that, with pH of 4.8, the steam condensate is undersaturated with calcium and ferrous ions, but it is saturated with silicic acid.

FIELD TEST

The purpose of the field test is to assess the corrosiveness and the deposition tendency of the Darajat geothermal fluids. To achieve these objectives, a simple series of materials testing procedures have been designed to measure surface corrosion rates, to check for localized and stress corrosion, and to determine scaling rates. Four different geothermal fluids were tested for their corrosiveness and scaling tendency, namely : (1) the raw steam, (2) the water separated from the steam, (3) the liquid phase condensed from the separated steam, and (4) the aerated liquid phase condensed from the separated steam.

Two methods of corrosion testing were used, i.e., the weight-loss (coupon) method and the electrical resistance method. Corrosion coupons were used to detect the occurrence of localized corrosion and to obtain long term average corrosion rates. To investigate stress corrosion stressed coupons were utilized, while scaling tendency was determined by using perforated scale coupons. The electrical resistance "corrosometer" was selected as continuous corrosion sensing device. Converting the change in the resistance measurements into known amounts of metal loss, data on corrosion rates were collected daily.

The engineering materials that were tested for their corrosion resistance in the four different geothermal fluids include:

AISI-1018	Carbon steel
AISI- 304	Austenitic stainless steel
AISI- 316	Austenitic stainless steel
AISI- 410	Martensitic stainless steel
	Inconel
	Titanium
	Aluminum

The corrosion coupons as well as the electrical resistance probes of these materials were obtained from Rohrback Cosasco Systems (USA). The tests were conducted for a period of 92 days extending from March 23 to June 23, 1989.

TEST RESULTS

The test results to be presented consist of four main topics, namely : (1) corrosion rate measurements, (2) localized corrosion and pitting, (3) stress-enhanced corrosion, and (4) scale deposition. Each of the topics will be discussed separately in the following paragraph.

1. Corrosion Rate Measurements

Results of the corrosion rate measurements for the seven different materials in the four different geothermal fluids are presented in Table-2. In each case, two corrosion rates are given, i.e., rates measured by the electrical resistance method and rates obtained from the weight-loss method for the duration of 92 days. The latter represents the long term average corrosion rates.

When readings from the corrosion probes showed two or more corrosion rates at different period of testing, then the higher rate is selected. Generally, as indicated by the test results, the corrosion rates obtained from the coupons closely agree with the electrical resistance readings if the probe measuring element of that particular material showed one constant rate during the entire test period.

(a). Corrosion rates in steam

Almost all materials tested in this environment exhibit two corrosion rates with the lower rate occurring in the second half of the test period. For the two austenitic stainless steels and Inconel, their corrosion rates decreases to a very low value of 2-3 mpa near the end of the test campaign. The lower corrosion rate of the carbon steel is 25 mpa, while for aluminum its lower value is 90 mpa. Corrosion rate readings from titanium probe indicates that this metal was not affected by the corrosivity of the steam environment.

(b). Corrosion rates in separated water

Contrary to the results found in the steam phase, titanium in the separated water environment showed a distinct corrosion rate of 31 mpa. Carbon steel exhibits a changing behavior in this test condition. A very low corrosion rate of carbon steel in the first half of the test period indicates that it has a strong corrosion resistance, but this rate subsequently increases to 27 mpa as the test progressed. Rate readings from the aluminum probes not only indicate a high corrosion rate but also exhibit a nonlinear increase in the resistance of the probe element, suggesting the possible occurrence of pitting.

(c). Corrosion rates in steam condensate

In this environment carbon steel again experienced a change in the corrosion rate. Initially the rate was roughly 250 mpa, but it

doubled at the end of the test period. Similarly AISI-316 austenitic stainless steel showed a moderate corrosion rate in the second half of the exposure period, while initially it displayed a strong corrosion resistance. Close agreement between the two differently obtained rate values is demonstrated by AISI-304 austenitic stainless steel in this test condition. Rate readings from its probe revealed that it has only one corrosion rate during the entire test campaign. Corrosion rate for aluminum could not be determined because its corrosion probe gave unreliable data.

(d). Corrosion rates in aerated condensate

Except the two austenitic stainless steel, almost all materials suffered from the increased corrosivity of the aerated test condition. Carbon steel and aluminum, in particular, experienced a significanf increase in their corrosion rates. Even though AISI-410 martensitic stainless steel in this environment corrodes at a rate of 41 mpa in the second half of the test period, it showed strong corrosion resistance in the early weeks of testing.

2. Localized Corrosion and Pitting

To observe localized corrosion and pitting attack, coupons of the weight-loss method were utilized in this corrosion test. Coupons of the seven different types of materials were exposed to the four different geothermal fluids for one, two, and three months. No distinct sign of localized corrosion was detected in any of the exposed coupons.

Some probe element types, typically wire or tube, may also be used to determine the presence of pitting attack. Pitting can cause a nonlinear increase in the resistance of the measuring element exposed to corrosive environment. In spite the fact that the resistance of the aluminum element tested under separated water environment increased nonlinearly, no macroscopic pits was observed on the aluminum coupon exposed to the same condition.

3. Stress-enhanced Corrosion

U-bend specimens were used in this test to determine the presence of stress-enhanced corrosion. Of all the materials tested in the four different environment, none suffered from stress corrosion cracking, i.e., no cracks was detected, after being exposed for one, two, and three months.

4. Scale Deposition

To investigate the possible presence of scale deposition, scale coupons drilled with a series of different sized holes to collect deposits were installed. The strength of the scaling tendency is determined by the largest size hole that has accumulated deposit.

In each of the four geothermal fluids, three scale coupons were exposed. The coupons were retrieved periodically at one-month interval during the three months test campaign. The results indicate that the strength of the scaling tendency was highest in the aerated steam condensate with only the smallest hole collecting deposits after three months of exposure. Unfortunately scaling rate determination was inconclusive.

DISCUSSIONS

The uniform corrosion rates in the seven different materials, as detailed in Table-2, are low to moderate except for AISI-1018 carbon steel and aluminum. Carbon steel experienced very severe corrosion in the steam condensate and in the aerated steam condensate, while aluminum may well suffered very severe corrosion rates in all the four tested geothermal fluids. Considered to be the "workhorses" for the process industries, the austenitic stainless steels AISI-304 and AISI 316, on the other hand, exhibit excellent corrosion resistance with low corrosion rates in any of the four media.

The high corrosion rates of carbon steel in the uncontaminated and in the aerated steam condensate raised some concern because the corrosion product may likely be its ferrous ions, as detailed by Figure-2, capable of increasing the ferrous ion concentration. Referring to Figure-6, however, it seems unlikely that the increased ferrous ion concentration will result in the precipitation of $FeSiO_3$ at low pH 'values.

The corrosion rate of carbon steel in the separated water environment is moderately low, and the corrosion product is likely to be solid FeS_2 or Fe_2O_3 as depicted in Figure-1. Although Figure-5 indicates that the ferrous ion concentration in the separated water is near saturation with respect to $FeSiO_3$, the low corrosion rate and the state of the corrosion product will probably create a limited effect to the increase of the ferrous ion concentration.

Figure-3 and Figure-5 of the separated water as well as Figure-4 and Figure-6 of the steam condensate illustrate the remote probability of calcium precipitating as calcite or calcium silicate because the calcium ion concentration in both media is undersaturated.

Even though findings based on calculated results suggest the imminent condition for FeSiO and silica to precipitate, test results from the scale coupons indicate that the strength of the scaling tendency in general is minimal.

CONCLUSIONS

1. Except AISI-1018 carbon steel and aluminum, the corrosion rates of the tested materials are low to moderate with a noticeably higher rates in the aerated condition.

2. The austenitic stainless steels AISI-304 and AISI-316 demonstrate strong corrosion resistance and can withstand satisfactorily the deleterious effects of the four geothermal fluids.

3. No localized corrosion or pitting was visually detected in this study.

4. Not one of the seven tested materials gave indication of suffering from stress corrosion cracking

5. The strength of the scaling tendency is found to be minimal, with a probability of silica and ferrous silicate as the deposited compounds.

ACKNOWLEDGEMENTS

The author wishes to express his thanks to Amoseas Indonesia Inc. for providing support in financing the field tests, and to PERTAMINA in granting permission to publish the test data.

Table - 1

Chemical Composition of the Darajat Geothermal Fluids

COMPOSITION	SEPARATED WATER			STEAM CONDENSATE		
	max	min	ave	max	min	ave
1. Cations [mg/lt]						
Na^+	24.4	0.2	3.1	1.8	< 0.1	0.5
K^+	3.4	0.3	0.9	0.4	0.1	0.2
Ca^{++}	15.3	0.2	3.2	15.0	< 0.1	1.5
Mg^{++}	1.5	C 0.1	0.4	0.1	< 0.1	0.1
NH_4^+	9.0		5.8	4.25	-	2.3
Li^+	0.1		0.05	< 0.1	-	0.1
Fe total	387.12	0.38	55.3	62.4	2.99	15.0
Al^{+++}	0.35		0.2	0.24	-	0.1
cs+	< 0.01		< 0.01	< 0.01		0.01
2. Anions [mg/lt]						
HCO_3^-	35	nil	15.6	35	15	24
$CO_3^=$	nil	nil	nil	nil	nil	nil
Cl^-	23	nil	4.8	5	nil	1.4
$SO_4^=$	806	< 1	119	145	nil	25
F^-	1.3		0.5	0.23	0.10	0.13
Br^-	0.5		0.3	1.0	0.1	0.5
[mg/lt]						
4. SiO_2	30	2	12	25	0.1	4.3
5. B	49.3	4.9	31.5	15.4	0.12	2.8
6. As	0.16	0.01	0.07	0.16	0.01	0.05
7. H_2S	106.9	0.1	29.8	84.6	1.1	52.8
8. Diss. CO_2	551	54	274	408	78	226
9. pH (25°)	5.28	3.80	4.5	5.28	4.28	4.8

Table - 2

The Corrosion Rates of the Tested Materials

MATERIALS		Steam		Separated Water		Condensate		Aerated Condensate	
		Probe	Coupon	Probe	Coupon	Probe	Coupon	Probe	Coupon
AISI-1018	Carbon Steel	30.23	58.0	26.92	86.0	489.71	242.9	3048	360.9
AISI- 304	Austenitic S.S.	27.18	0.5	5.33	0.8	1.02	0.9	0.76	0.7
AISI- 316	Austenitic S.S.	6.35	0.8	2.89	0.8	13.21	0.9	1.27	0.5
AISI- 410	Martensitic S.S.	20.07	4.3	10.92	10.9	11.68	5.7	40.64	10.2
	INCONEL	17.02	4.9	1.78	4.6	2.03	8.5	5.08	21.0
	TITANIUM	0.0	0.2	31.24	0.6	5.84	0.1	12.7	1.5
	ALUMINUM	558.04	14.7	633.73	22.1	n.o.	10.1	n.o.	77.1

n.o. = not observed
Units in micrometer per annum (mpa)

REFERENCES

Barner,H.E. and Scheuerman,R.V., 1978. Handbook of Thermochemical Data for Compounds and Aqueous Species. Wiley-Interscience, New York.

Biernat,R.J. and Robins,R.G., 1972. High-temperature Potential-pH Diagrams for the Iron-Water and Iron-Water-Sulphur Systems. Electrochim. Acta, 17: 1261-1283.

Cobble,J.W., Murray,Jr.,R.C., Turner,P.J., Chen,K., 1982. High Temperature Thermodynamic Data for Species in Aqueous Solution. EPRI-NP-2400, Res.Proj. 1167-1, Electric Power Research Institute, Palo Alto (USA).

Garrels,R.M. and Christ,C.L., 1965. Solution, Minerals, and Equilibria. Freeman Cooper & Co., San Francisco.

Henley,R.W., Truesdell,A.H., Barton,Jr.,P.B. and Whitney,J.A., 1985. Fluid-Mineral Equilibria in Hydrothermal Systems. Review in Economic Geology, vol. 1, Soc. of Economic Geologists.

Stumm,W. and Morgan,J.J., 1970. Aquatic Chemistry, Wiley-Interscience, New York.

Wilson,P.T. and Lichti,K.A., 1982. Assessment of Corrosion Performance of Construction Materials in Geothermal Steam. Proc. Pacific Geothermal Conf., 185-190.

ARAGONITE DEPOSITED FROM BR6 DISCHARGE; 1972.
Photo: D. L. Homer, NZ Geological Survey.